

Article

Studies on Biobased Non-Isocyanate Polyurethane Coatings with Potential Corrosion Resistance

Nikhil Dhore ^{1,†} , Ermiya Prasad ^{1,2,†}, Ramanuj Narayan ¹, Chepuri R. K. Rao ^{1,*} and Aruna Palanisamy ^{1,*} 

¹ Polymers and Functional Materials Department, CSIR—Indian Institute of Chemical Technology, Hyderabad 500007, India

² Academy of Scientific and Innovative Research (AcSIR), Ghaziabad 201002, India

* Correspondence: ramchepuri@iict.res.in (C.R.K.R.); aruna@iict.res.in (A.P.)

† These authors contributed equally to this work.

Abstract: This work deals with the development of non-isocyanate polyurethane (NIPU) composites with an aniline oligomer, viz., tetraniline (TANI) for corrosion-resistant coatings. Firstly, epoxidized-soyabean oil was converted to carbonated oil by inserting CO₂ under high temperature and pressure into the epoxy ring. Then, varying weights of oligoaniline—0.5, 1, 2 and 4 wt % (based on the weight of CSBO)—were added to CSBO and cured with tetraethylenepentamine (TEPA, 25 wt % based on CSBO) at 80 °C for 12–15 h. The effects of oligomer loading on the thermal, mechanical and surface wetting properties of the free standing films were studied. The ATR-FTIR spectra of the films exhibited peaks corresponding to the bis-carbamate linkages, confirming the formation of urethane linkages. TGA analysis showed that the addition of oligoaniline did not alter the initial degradation temperature much; however, the residue increased with increasing loading of tetraniline. Both tensile strength and elongation (at break) increased with increasing oligoaniline content. While the glass transition temperature of the films was observed at approximately room temperature, i.e., 20–30 °C, for all the compositions, the contact angles of the composites were found to be less than that of the bare NIPU films. However, all the compositions were hydrophobic, exhibiting contact angles in the 98–110° range. SEM analysis of the cross-sections of the films confirmed the uniform distribution of tetraniline particles and surface morphology showed that the roughness increased with the loading of tetraniline from 0.5 to 4%. MS panels coated with NIPU exhibited good barrier properties and as loading of TANI increased, the rate of corrosion decreased. Salt spray tests indicated that oligoaniline improved the adhesion of the coating to MS and corrosion resistance compared to the neat NIPU coating.

Keywords: carbonated soyabean oil; NIPU; oligoaniline; corrosion resistance



Citation: Dhore, N.; Prasad, E.; Narayan, R.; Rao, C.R.K.; Palanisamy, A. Studies on Biobased Non-Isocyanate Polyurethane Coatings with Potential Corrosion Resistance. *Sustain. Chem.* **2023**, *4*, 95–109. <https://doi.org/10.3390/suschem4010008>

Academic Editor: Matthew Jones

Received: 23 December 2022

Revised: 2 March 2023

Accepted: 6 March 2023

Published: 9 March 2023



Copyright: © 2023 by the authors. Licensee MDPI, Basel, Switzerland. This article is an open access article distributed under the terms and conditions of the Creative Commons Attribution (CC BY) license (<https://creativecommons.org/licenses/by/4.0/>).

1. Introduction

Biobased coatings are gaining importance due to strict environmental legislations such as restrictions on VOC emission and the need for biodegradability. In addition, depleting fossil fuel resources have now driven both academic and industrial research towards utilization of natural resources for developing novel materials which can substitute petroleum-based materials. Among the various renewable sources, vegetable oil is advantageous in terms of its availability, cost, functionality and performance. Soyabean oil has been widely used for several industrial applications in its epoxidized form as raw materials for coatings, co-plasticizer for PVC processing [1], pharmaceutical plastic packaging material [2], precursors for synthesis of acrylates [3], polyols [4] and more recently non-isocyanate PUs. ESBO is also used in coatings and adhesives [5] because of its low cost, strong photosensitivity, excellent coated film performance and low viscosity. Epoxidized soyabean oil is commercially available and it is less expensive, highly functional (with %oxirane oxygen content of approximately 6.5–7), colorless, odorless, and less viscous. It

has already been explored widely for applications in NIPU by first converting the epoxidized SBO to carbonated SBO by CO₂ insertion followed by opening of the 5-membered cyclic ring with amines at elevated temperatures to give a cross-linked network structure. Several groups have synthesized and evaluated CSBO-based NIPUs [6–11].

However, polymer films serve as coatings, especially as protective coatings when they carry an additive, which acts as a corrosion inhibitor. Many organic, inorganic and hybrid materials such as Zn Al polyphosphate and 2-mercaptobenzimidazole [12], tetraethyl orthosilicate (TEOS) [13], grafted graphene oxide nanosheets [14], perfluorooctylglycidyl ether [15], and zinc graphene oxides [16] have been reported to exhibit this activity. Anti-corrosion coatings based on NIPU were synthesized using amine-terminated NIPU (prepared from bisphenol A cyclic carbonate and fatty acid amine) and tetraethyl orthosilicate (TEOS). NIPU coating with 5 weight % of TEOS showed the best anti-corrosion behavior [13]. Perfluorooctylglycidyl ether (PFGE) was used to synthesize perfluorooctyl cyclic carbonate (PFGC), which in turn was used to prepare fluorine-containing NIPU coatings. The coatings exhibited good flexibility, adhesion, and impact resistance, very low water uptake, hydrophobicity and corrosion resistance [15]. A dual curable coating was achieved by curing of amine functional NIPU oligomers with 3-glycidylxypropyl trimethoxysilane followed by moisture curing at room temperature. The resulting coatings had enhanced flexibility and good corrosion in resistance [17]. Carbonated sunflower oil (CSFO)-based NIPUs were prepared by using 1,2-ethylenediamine, diethylenetriamine and isophorone diamine as curing agents. IPDA and EDA cured systems showed good properties (thermal, chemical, mechanical and anti corrosion). IPDA-based coating showed high corrosion resistance and lowest corrosion rate, which is attributed to its structure [18]. In another study, zinc oxide was treated with cyclic carbonate functional alkoxy silane and incorporated in NIPU formulations in varying amounts and coated on mild steel substrates. The nanocomposite coatings performed well even after 500 h of salt spray test compared to the bare-NIPU-coated panel. NIPU coatings containing 3% of ZnO (treated and untreated) had higher corrosion potential values compared to all other systems [19].

In the last decade, a great deal of work on electroactive polymers with application in various fields, viz., corrosion-resistant coatings, electroluminescent devices, electrochemical sensors, and electrostatic dissipation coatings have been carried out [20–26]. However, the major problem is processability issues. For instance, the polyaniline and N-methyl-2-pyrrolidinone (NMP) solution usually leads to the generation of gels. In addition, other electroactive polymers such as polythiophene and polypyrrole are not completely dispersible in the usual organic solvents. The focus of many researchers is on the well-defined structure of the electroactive oligomers to overcome the problems. Several groups have synthesized and characterized amine-terminated aniline trimer (ACAT) [27], aniline tetramer, pentamer and studied their redox properties [28]. Some groups have reported the oligoaniline-incorporated polyurethane [29], ACAT-based electroactive epoxy [30], polyimide [31], polyamide [32], and polyurea [33], etc.

In the present study, we have prepared NIPU–TANI nanocomposites containing varying amounts of TANI. The incorporation of the oligomer was anticipated to improve the (i) the adhesion of the coating to the MS substrate, (ii) the mechanical properties of the film, and (iii) the corrosion resistance of MS panels. Thus, an eco-friendly and highly functional coating was developed using epoxidized soyabean oil by a 100% atom economical route.

2. Material and Methods

2.1. Materials

Epoxidised soybean oil (ESBO specification: Table 1) was obtained from Makwell organic private limited, Mumbai, India. Tetraethylenepentamine (TEPA) was obtained from Sigma-Aldrich (St. Louis, MO, USA). Kosmos (stannous octoate) was purchased from Goldshmidt GmbH, Essen, Germany. Hydrobromic acid (HBr, 46%), acetic acid, hydrochloric acid (HCl), sodium chloride (NaCl), ammonium hydroxide (NH₄OH) and

tetrabutylammonium bromide (TBAB) were from Finar chemicals Pvt. Ltd. 4,4'-diamino-diphenylamine sulfate and N-phenyl-p-phenylenediamine were purchased from TCI.

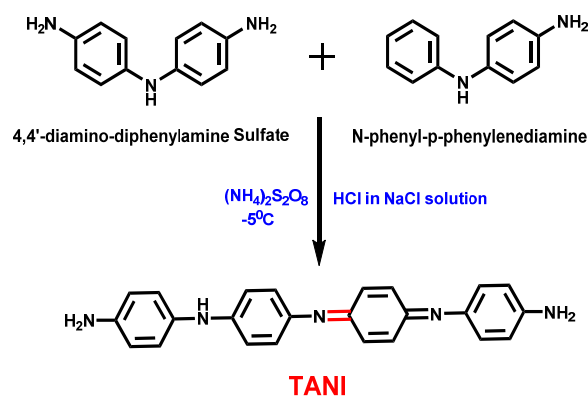
Table 1. Specifications of Epoxidized Soybean Oil (ESBO).

Characteristics	Specification
Appearance	Light yellow clear liquid
Specific gravity	0.987
Moisture content (%)	0.1%
pH	6.5
Oxirane oxygen content (%)	6.52
Acid value (mg KOH/g)	0.64
Iodine value (g I ₂ /100 g)	1.62

2.2. Methods

2.2.1. Synthesis of Tetraniline

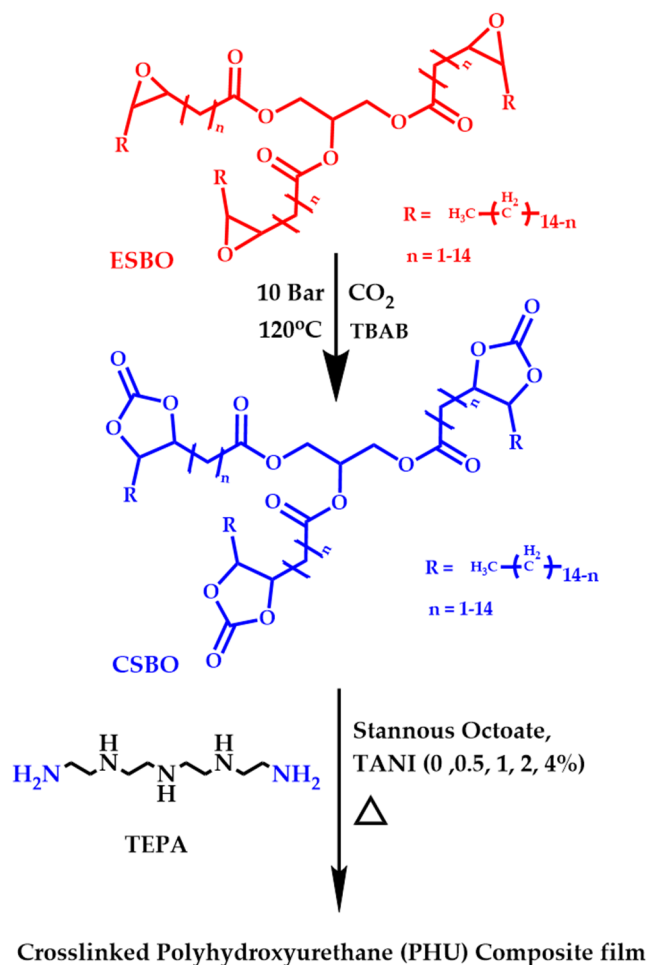
4,4'-diamino-diphenylamine sulfate (7 g, 0.023 mol) and N-phenyl-p-phenylenediamine (4.33 g, 0.023 mol) were dissolved in aq. HCl (1.0 molar, 300 mL) containing 23 g NaCl. Ammonium persulfate solution (5.306 g, 0.023 mol) in aqueous HCl (1.0 mol/L, 100 mL) was added dropwise to the above solution (5 mL/min) maintained at $-5\text{ }^{\circ}\text{C}$. The reaction mixture was stirred at $-5\text{ }^{\circ}\text{C}$ for 2 h and the resulting precipitate was collected by filtration, then washed with aq. HCl (1.0 molar, 300 mL) followed by distilled water. The precipitate was stirred for 1 h by adding 200 mL of 5 M NH_4OH solution, filtered and dried overnight in a vacuum oven at $50\text{ }^{\circ}\text{C}$. The resulting compound was characterized for its structure using ^1H NMR, FT-IR and mass spectroscopy (yield—80%, Scheme 1) [34].



Scheme 1. Synthesis of TANI.

2.2.2. Synthesis of Carbonated Soybean Oil

Carbonization of soybean oil was carried out in a high-pressure reactor (Amar Equipments Pvt. Ltd., Mumbai, India, 1 L Volume, -1 to 100 Bar Vessel Design Pressure and -10 to $250\text{ }^{\circ}\text{C}$ Vessel Design Temperature) as shown in Scheme 2. To the reaction vessel, approximately 250 g of ESBO and a catalytic amount of tetrabutyl ammonium bromide (TBAB, 8.8 weight %) were added with respect to the weight of ESBO. Then, the reaction mixture was heated to $120\text{ }^{\circ}\text{C}$ with continuous stirring. CO_2 was passed into the reactor, pressurized to 10 bar and the pressure was maintained during the entire course of reaction, i.e., for 24 h. After the completion of the reaction, clear and brownish viscous oil, CSBO, was collected and the sample (Figure 1) was subjected to epoxy value determination to confirm the conversion of epoxy to 5-membered cyclic carbonate ring. CO_2 insertion was also confirmed by IR, ^1H NMR and ^{13}C NMR.



Scheme 2. Synthesis of carbonated SBO and NIPU.



Figure 1. Images of ESBO and CSBO Resin.

2.2.3. Synthesis of NIPU and Its Composite

TEPA as a curing agent (25 weight % based on CSBO) and stannous octoate as a catalyst (2 weight % based on CSBO) were added to a given weight of CSBO. Varying amounts (0, 0.5, 1, 2, and 4%) of TANI were used in the formulation to enhance the corrosion resistance of the NIPU films. TANI was sonicated in DMF for 1/2 h, prior to mixing with CSBO and PETA. The blend was made by first mixing CSBO and TEPA for 5–6 min followed by the addition of sonicated TANI dispersion. The composites were casted in silicon mold and cured at 80 °C for 12–15 h.

2.3. Characterization of ESBO, CSBO and Cured Film

Epoxy value, iodine value and acid value were determined as per standard procedures (refer supplementary information).

2.3.1. Viscosity

The viscosity of ESBO and CSBO was determined using a strain-controlled rheometer (102 series modular compact rheometer, Anton Paar, Graz, Austria) using cone/plate geometry with an adjusted gap of 1 mm.

2.3.2. Fourier Transform Infrared Spectroscopy (FTIR)

Functional groups present in ESBO and CSBO were identified using a PerkinElmer (Spectrum 1000, Waltham, MA, USA) Fourier transform-infrared (FT-IR) spectrometer, where the material was smeared on the KBr pallets and IR recorded. Attenuated Total Internal Reflection (ATR) was used for recording the IR of the films (minimum 16 scans) in the 400–4000 cm^{-1} range.

2.3.3. Nuclear Magnetic Resonance Spectroscopy (NMR)

Nuclear Magnetic Resonance Spectroscopy (NMR) (^1H and ^{13}C) spectra were recorded using a Varian-Inova400 MHz spectrometer in DMSO- d_6 (TANI) and a CDCl_3 (CSBO) solution in which tetramethylsilane (TMS) was used as an internal standard.

2.3.4. Electrospray Ionization Mass Spectroscopy (ESI-MS)

Electrospray Ionization Mass (ESI-MS) spectra were used to interpret the molecular weight of TANI, carried out on FINNIGAN LCQ Advance Max in methanol solution.

2.3.5. Water Contact Angle Analysis

The effect of TANI on the wettability of NIPU-coated films was evaluated using G10 Goniometer (KRUSS instrument, Hamburg, Germany) through sessile drop.

2.3.6. Thermogravimetric Analysis (TGA)

TGA was carried out using 5–10 mg of sample on a TA Q500 (TA Instruments, New Castle, DE, USA) thermogravimetric analyzer under N_2 atmosphere at room temperature to 600 $^\circ\text{C}$, with a 10 $^\circ\text{C}/\text{min}$ heating rate and the sample weight ranged from 5 to 10 mg.

2.3.7. Dynamic Mechanical Thermal Analyzer (DMA)

A DMA (TA Q800) was used to interpret the storage modulus (E') and glass transition temperature (T_g) of films at 1 Hz frequency in the multi-frequency-strain mode in the temperature range -50 to 80 $^\circ\text{C}$ at a heating rate of 10 $^\circ\text{C}/\text{min}$.

2.3.8. The Universal Testing Machine (UTM)

The mechanical properties of the coatings were evaluated by a universal testing machine (UTM) DAK-7200, India system, with a speed of 10 mm/min with a load cell and gauge length of 100 kg and 50 mm, respectively, according to ASTM D882. The specimens for UTM (micro tensile specimens) had the following dimensions: thickness 0.7 mm, width and length nearly 10 and 80 mm, respectively.

2.3.9. Scanning Electron Microscope

NIPU films containing oligoaniline were analyzed for their morphology using scanning electron microscope (SEM), Hitachi-S520 (Oxford link ISISSEM model), Tokyo, Japan. Cross-sections of the films were also scanned.

2.3.10. Tafel Polarization

Anti-corrosion performance TANI-loaded NIPU coated on the mild steel ($3 \times 3 \text{ cm}^2$) was assessed by Tafel polarization using an AUTOLAB electrochemical system (Potentiostat & Galvanostat, Metrohm, Netherlands) with an electrolyte (3.5% NaCl Solution) at room temperature.

2.3.11. The Salt Spray Fog Test

The coated MS panels were evaluated for corrosion resistance as per the ASTM B-117 salt spray fog test (Komal Scientific Pvt. Ltd., Mumbai, India). Cross-cuts were made on the coated surface to perceive the protective action on the coated panel. The coated panels were kept in a salt spray chamber and atomized using a 5% salt solution in water for 144 h.

3. Results and Discussion

3.1. Characterization of TANI

FTIR spectra (Figure 2A) exhibited a peak at approximately 3433 cm^{-1} assigned to the terminal NH_2 groups of TANI. In addition, the bands at 1593 and 1499 cm^{-1} could be related to quinoid and benzenoidring vibration. In NMR (Figure 2B), signals at 5.14 ppm are related to the proton of the primary amine. Peaks between 6.4 and 7.5 ppm are mainly related to the quinoid and benzenoidrings present in TANI. Further structure confirmation by HRMS (Figure 2C) showed a molecular ion peak at 380.18 ($M+1$) matching with TANI molecular weight. From these spectroscopic data, the structure of TANI was confirmed [34].

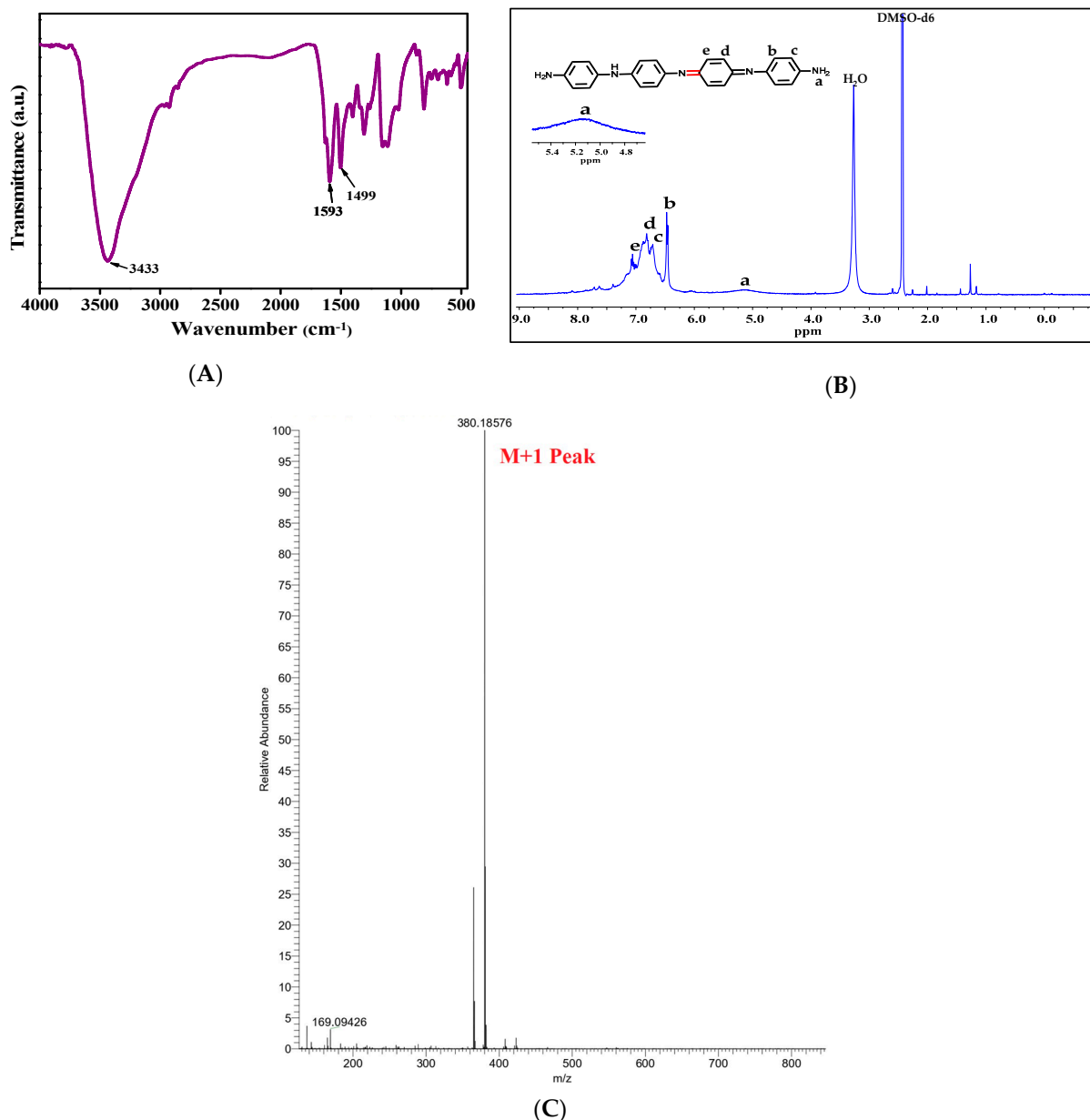


Figure 2. (A) FTIR, (B) Mass and (C) NMR Spectra of TANI.

3.2. Characterization of CSBO

The physicochemical properties of the carbonated soyabean oil is listed in Table 2. Since oxirane oxygen content has dropped from 6.5 to 0.55, the insertion of CO₂ into the epoxy ring has been confirmed. Figure 3 shows the IR spectra of epoxidized and carbonated soyabean oil. The peak at approximately 842 cm⁻¹ in the ESBO spectrum corresponds to the epoxy groups, which have completely disappeared in the CSBO and a new peak corresponding to the C-O and C-H stretching at the alpha-position of carbonate appear at approximately 1806, 1054, and 870 cm⁻¹, respectively. Further, conversion of epoxy rings into cyclic carbonate was confirmed by ¹H and ¹³C NMR spectroscopy. The appearance of the new peaks in CSBO at approximately 4.4–4.9 ppm in Figure 4 is related to protons of the cyclic carbonate rings, while the epoxy ring protons have almost disappeared (2.8–3.2 ppm). In the ¹³C NMR (Figure 5), one can observe the new peak at 154 ppm and 79–82 ppm corresponding to the carbon atom of the cyclic carbonate moiety.

Table 2. Physicochemical Properties of the CSBO.

Properties	Value
Viscosity (cPs) @44 °C	10,180
Moisture Content (%)	0.31
Appearance	Brownish viscous liquid
Oxirane Oxygen Content (%)	0.55

3.3. Characterization of NIPU Composites

CSBO was formulated with varying amounts of TANI (0.5, 1, 2 and 4 wt % based on the CSBO) using 25 wt % TEPA (based on the CSBO). TANI was dissolved in the DMF by sonication for 1/2 h, then mixed with CSBO, TEPA and the catalyst in order to achieve homogeneity of TANI in the resin. This mixture was then poured into a mold and cured in the oven overnight (12–15 h). The solid content in the composite was maintained at approximately 65%, which can be considered as high solid coatings. The cured films with different amounts of TANI are shown in Figure 6. The formation of urethane linkages in cured polyhydroxyurethane films was confirmed by ATR-FTIR.

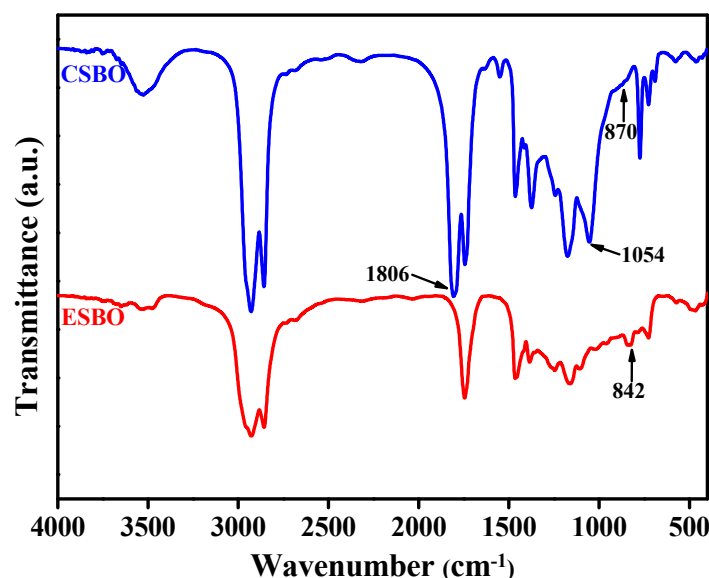


Figure 3. FTIR Spectra of ESBO and CSBO.

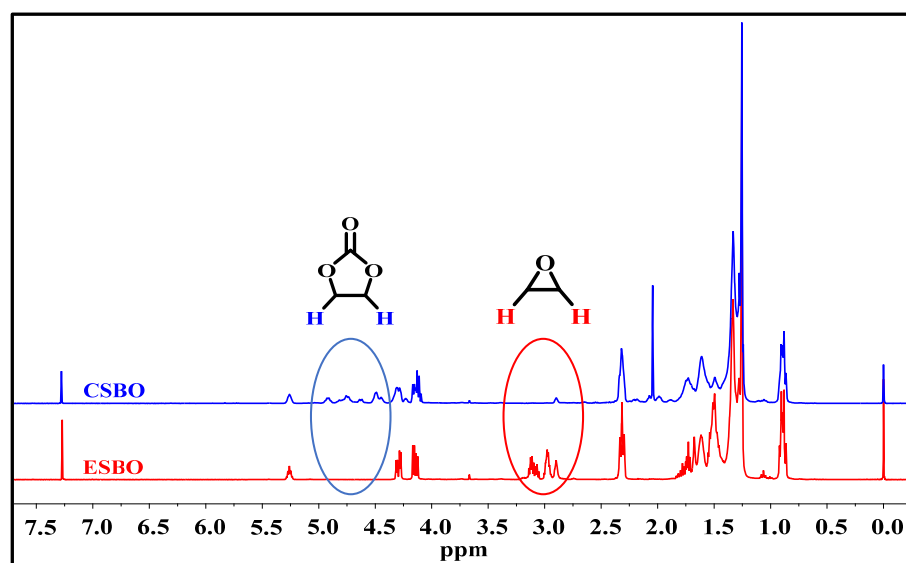


Figure 4. ^1H NMR of ESBO and CSBO.

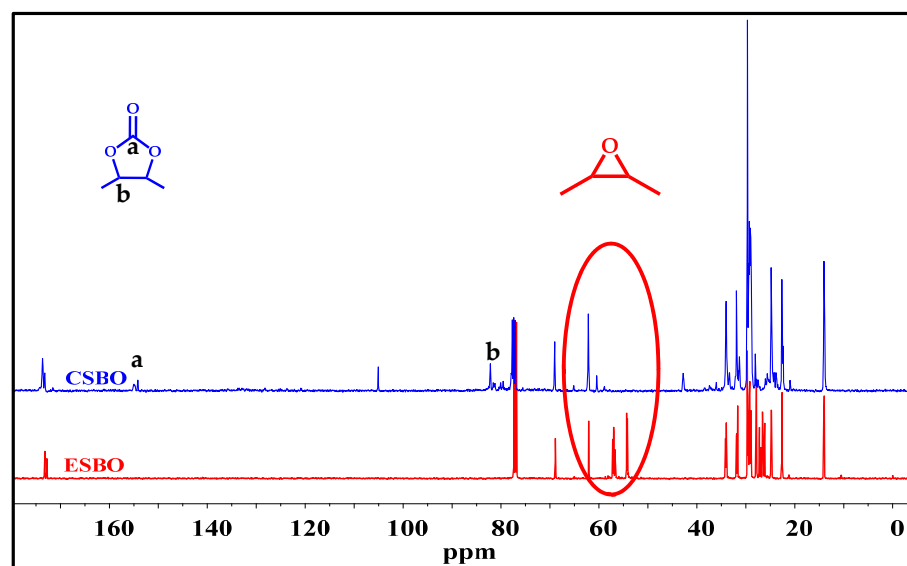


Figure 5. ^{13}C NMR of ESBO and CSBO.

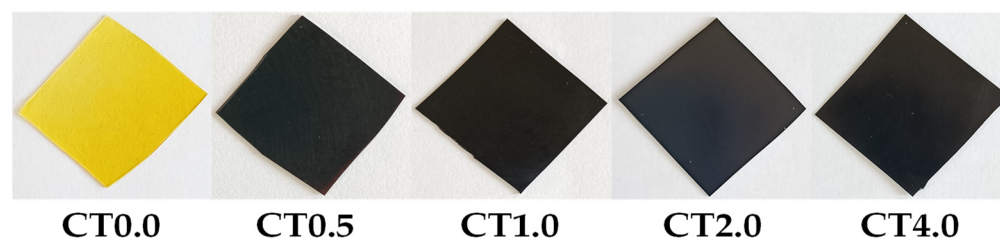


Figure 6. Cured Polyhydroxyurethane–TANI Composites.

3.3.1. Fourier Transform Infrared Spectroscopy of NIPU–TANI Composites (FTIR)

The ATR-FTIR spectra show peaks related to the formation of the urethane linkages (Figure 7). NH stretching and bending peaks appear at 3326 and 1531 cm^{-1} , respectively. The peaks at 1695 and 1705 cm^{-1} are attributed to the $\text{C}=\text{O}$ stretching of the urethane bond. Hence, ring opening of cyclic carbonate with amines leading to urethane bond formation is confirmed.

3.3.2. Thermal Properties

The TGA analysis of NIPU composite films was carried to understand its thermal stability and degradation trend with respect to the temperature increase from 30 to 600 °C at a rate 10 °C/min. The initial degradation from 180 to 265 °C may be related to the dissociation of urethane linkages while weight loss from 266 to 440 °C may correspond to decomposition of the long alkyl chains of soyabean oil. Thermal degradation of the polymeric chain due to C–C and C–O bond scission occurs at approximately 440–520 °C. The 5% and 50% degradation temperature (T_d) of the different composite film are shown in Table 3 and it was observed that there is no effect of TANI loading on the thermal stability of NIPU coatings. It was observed that the % residue of the composite film at 550 °C increased with TANI loading.

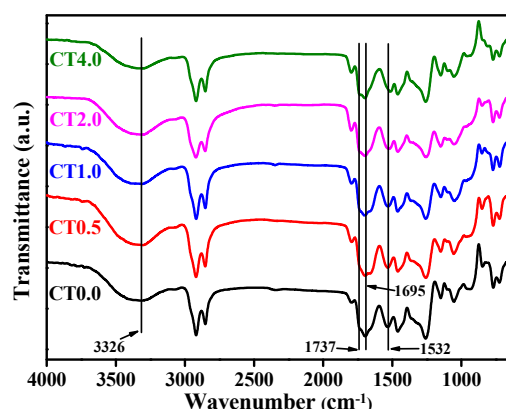


Figure 7. ATR-FTIR of NIPU Composite Film.

Table 3. Thermal Degradation Data of NIPU Composites.

Sample Code	Degradation Temperature (°C)		
	5% T_d	50% T_d	Residue @550 °C (%)
CT 0.0	207	373	1.72
CT 0.5	185	373	2.11
CT 1.0	204	372	1.40
CT 2.0	203	372	2.86
CT 4.0	196	382	4.14

3.3.3. Thermomechanical Properties

Dynamic mechanical thermal analysis (DMA) was used to determine the dynamic viscoelastic properties and glass transition temperatures (T_g) of the films. Figure 8A shows a variation in the storage modulus (E') with respect to the temperature and the $\tan \delta$ vs. temperature plot (Figure 8B) shows the T_g values. The thermomechanical parameters of the cured composite films are tabulated in Table 4. The storage modulus vs. temperature profiles of the NIPU and NIPU TANI composites are shown in Figure 8A. It was observed that the composites have a lower storage modulus compared to the bare NIPU film, which may be due to the effect of TANI on the extent of H bonding in the NIPU backbone due to the presence of NH groups in the oligoaniline backbone. The glass transition temperature, as observed from the peak of the $\tan \delta$ curves of the composites, was slightly higher than the bare NIPU films as a result of the reinforcing effect of TANI. The curves also became much narrower with TANI loading, which shows that the oligoaniline is reducing the extent of physical cross-linking within the NIPU chains. The broadest curve was observed for CT 0.0, where TANI is completely absent, hence H bonding comes into the picture, leading to physical cross-links. Generally, the higher the extent of cross-linking (either

chemical or physical), the broader the $\tan \delta$ peak. In general, the peak area of $\tan \delta$ curves shows the energy dissipation capability of materials [35].

3.3.4. Static mechanical Properties

The effect of TANI addition on the mechanical properties of the NIPU films was evaluated using the universal testing machine (UTM). The tensile strength and the percentage of elongation at break of the NIPU composite are compiled in Table 4. All the composite films show elastic behavior as observed from the stress vs. strain curve (Figure 9). It was observed that TANI-incorporated films had a higher tensile strength and elongation compared to the bare NIPU films. This may be due to the reinforcing effect of TANI on the PU matrix. However, the optimum loading for maximum strength and elongation was found to be 1%, beyond which both the strength and the elongation (%) dropped.

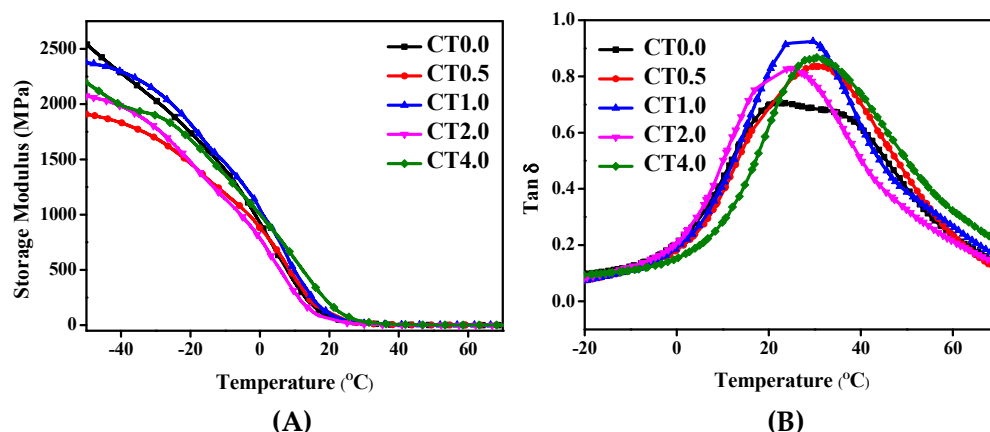


Figure 8. (A) Storage Modulus vs. Temperature and (B) $\tan \delta$ vs. Temperature Curves.

Table 4. Dynamic Mechanical and Static Mechanical Properties of the Composite Films.

Sample	Storage Modulus (MPa)		T_g ($^{\circ}\text{C}$)	Tensile Strength (MPa)	Elongation (%)
	@ -50 $^{\circ}\text{C}$	@ 25 $^{\circ}\text{C}$			
CT 0.0	2543	30	21.44	0.45 ± 0.10	36.71 ± 3.1
CT 0.5	1910	29	29.78	0.85 ± 0.06	89.16 ± 0.7
CT 1.0	2377	35	26.92	0.97 ± 0.07	92.00 ± 4.0
CT 2.0	2071	18	24.54	0.57 ± 0.08	44.75 ± 4.3
CT 4.0	2198	73	29.33	0.75 ± 0.08	61.6 ± 5.0

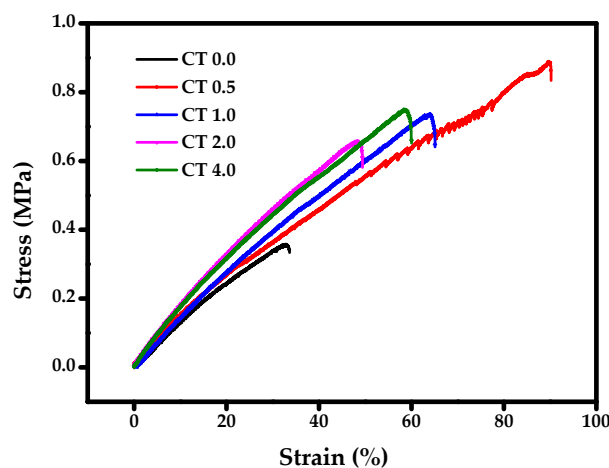


Figure 9. UTM Plot of NIPU Composite Films.

3.3.5. SEM Analysis

Scanning electron microscopy was employed to study the surface morphology and the cross-sectional morphology of the NIPU composite. As shown in Figure 10A, surface roughness increased with the increase in TANI loading and the surface had a microporous flake-like structure. The cross-sectional images (Figure 10B) confirm that TANI is well dispersed in the NIPU matrix even at higher loading (4%).

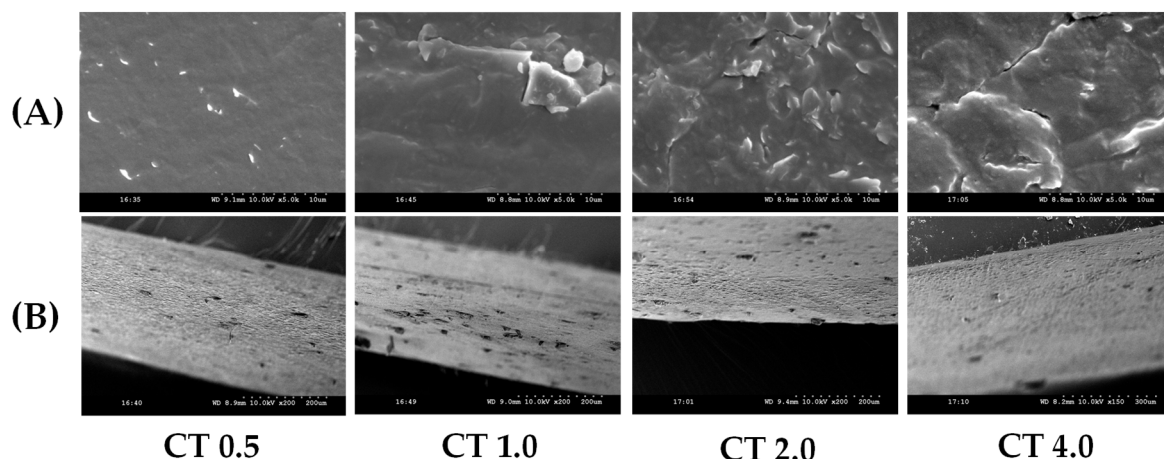


Figure 10. SEM Images: (A) Surface Morphology and (B) Cross-Section of NIPU Composite Films.

3.3.6. The Water Contact Angle

The surface wettability characteristics of the composite films (water contact angle) coated on glass surfaces were evaluated by using a KRUSS goniometer (Figure 11). Basically, a material is said to be hydrophilic if the water contact angle (WCA) is less than 90° , and hydrophobic if it is greater than 90° . It was noticed in the present case that all the films exhibited a hydrophobic nature. However, addition of TANI reduced the water contact angle by approximately 12° to 7° . While NIPU without TANI shows hydrophobic behavior due to the presence of long alkyl groups of the triglyceride units in soybean oil, addition of TANI induced surface roughness (as seen in SEM images) and also hydrophilicity in the PU matrix.



Figure 11. WCA of NIPU Composite Films.

3.3.7. Polarization Studies

Tafel polarization measurement is a technique for analyzing the anti-corrosive properties of polymeric coatings by evaluating the current vs. potential. By this technique, corrosion current (I_{corr}), corrosion potential (E_{corr}) and corrosion rate (C_R) on the metal panels were measured [36–38]. I_{corr} and E_{corr} will give bisecting extrapolated lines from both the oxidation and reduction parts. The Tafel study (Figure 12 and Table 5) of NIPU coated on the mild steel panel ($3 \times 3 \text{ cm}^2$) demonstrated that as loading of TANI increased, the rate of corrosion decreased. E_{corr} values of the coated NIPU panel shifted more towards positive anodic values compared to that of the bare MS panel, which substantiates the superior control of the reaction (anodic and cathodic) because of barrier properties of NIPU coatings. CT 0.0 panel without TANI has showed a corrosion rate of $2.69 \times 10^{-4} \text{ mm/year}$ with a polarization resistance of $5.59 \times 10^3 \text{ k}\Omega$ while NIPU with TANI loaded showed a

lower corrosion rate with higher polarization resistance. With 4% loaded TANI, the C_R was 1.67×10^{-5} mm/year with a high polarization resistance of 73.80×10^5 k Ω . This trend suggested that TANI reduced the corrosion rate of mild steel with its redox behavior [39].

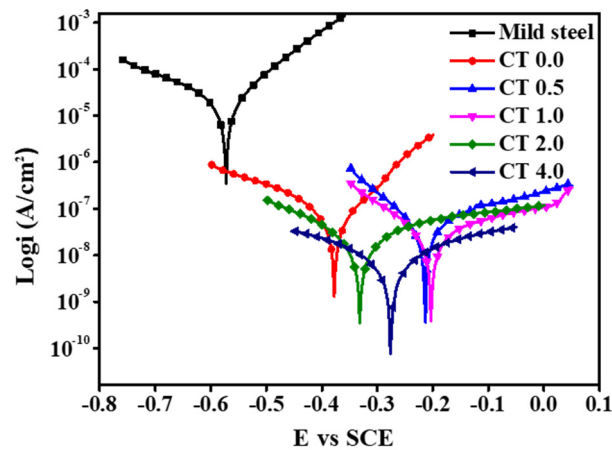


Figure 12. Tafel Polarization Plot of NIPU and its Composite Films.

Table 5. Tafel Polarization Data of NIPU Composite Films.

Sample	E_{Corr} (mV)	I_{Corr} (nA)	Corrosion Rate (C_R) (mm/year)	Polarization Resistance (Ω)
CT 0.0	−377.3	23.19	2.69×10^{-4}	5.59×10^5
CT 0.5	−213.66	11.99	1.39×10^{-4}	9.09×10^5
CT 1.0	−203.06	7.97	9.26×10^{-5}	15.39×10^5
CT 2.0	−331.08	5.8	6.81×10^{-5}	25.22×10^5
CT 4.0	−276.09	1.43	1.67×10^{-5}	73.80×10^5

3.3.8. The Salt Spray Fog Test

The salt spray fog test helps to investigate the spread of damage by way of the delamination or mechanical failure of the coating. Figure 13 displays the images of the coated panels after 144 h of exposure to salt spray (5% NaCl solution). The salt spray fog test result showed that the coating without TANI started to delaminate early while the TANI composite-coated panel showed good adhesion and corrosion resistance (Figure S1, SI). With increasing TANI, the adhesion of the coating to the panel increased and CT4.0 had the best adhesion and corrosion resistance. This correlates well with the polarization studies, where CT4.0 exhibited the highest polarization resistance and the lowest corrosion rate, 1.67×10^{-5} mm/year.

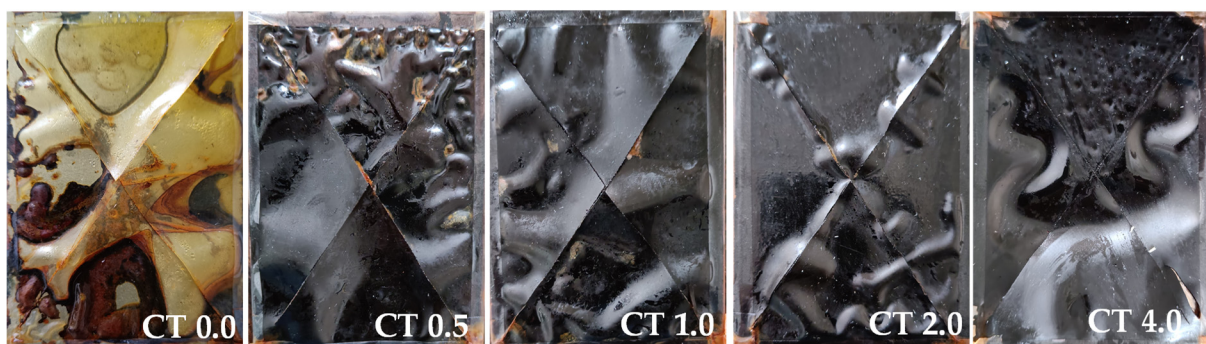


Figure 13. Salt Spray Fog Test Panels (144 h) of NIPU Composite Films.

4. Conclusions

A biobased non-isocyanate free polyurethane was synthesized from carbonated soybean oil using tetraethylenepentamine (TEPA) as a curing agent. Varying amounts of TANI (0.5, 1.0, 2 and 4%) were loaded into the PU matrix to induce corrosion resistance. It was observed that ATR-FTIR of the films exhibited peaks corresponding to the urethane linkages, thus confirming the formation of the polyhydroxyurethanes (PHU). TGA showed that the loading of oligoaniline did not affect the initial degradation temperature much because the dissociation of the biscarbamate linkages is the rate-determining step during the decomposition. Even though there was not a specific trend, the glass transition temperature of the films (from dynamic mechanical studies) increased with the incorporation of tetraniline, while the $\tan\delta$ peaks became more intense and narrower, indicating the effect of the oligoaniline on the extent of H bonding between the PU chains. TANI-incorporated films had better tensile properties than the bare NIPU, indicating the reinforcing nature of TANI, and composition with 1% TANI loading had the highest tensile strength and elongation. SEM images showed the uniform distribution of TANI particles accompanied with the increase in surface roughness with increasing TANI content. Further, the incorporation of oligoaniline led to a reduction in the water contact angle of the NIPU–TANI films due to the above reason. The corrosion resistance of the MS panels, as evaluated by polarization studies, improved with incorporation of TANI and CT 4.0 exhibited the best performance. The corrosion data were further substantiated by salt spray analysis, wherein TANI increased both the adhesion properties as well as the corrosion resistance compared to bare NIPU coatings.

Supplementary Materials: The following supporting information can be downloaded at: <https://www.mdpi.com/article/10.3390/suschem4010008/s1>.

Author Contributions: Conceptualization, A.P. and C.R.K.R.; methodology, A.P.; Validation, A.P. and C.R.K.R.; Formal analysis, N.D. and E.P.; investigation, N.D. and E.P.; resources, R.N.; writing—original draft preparation, N.D. and A.P.; writing—review and editing, A.P. and C.R.K.R.; visualization, A.P.; supervision, R.N. and A.P., project administration, R.N.; funding acquisition, R.N. All authors have read and agreed to the published version of the manuscript.

Funding: This research was funded by the Centre of Excellence (CoE) on Polymer Coatings for Protective, Decorative & Strategic Applications, which is granted by Department of Chemicals & Petro-chemicals Ministry of Chemicals & Fertilizers, Govt. of India, under project code GAP-0875 at the CSIR-Indian Institute of Chemical Technology, India.

Institutional Review Board Statement: Not applicable.

Informed Consent Statement: Not applicable.

Data Availability Statement: Data sharing not applicable.

Acknowledgments: N.D. would like to thank the Centre of Excellence on Polymer Coatings for Protective, Decorative & Strategic Applications at CSIR-IICT, Hyderabad fellowship. E.P. acknowledges CSIR for a senior research fellowship to pursue doctoral studies and is grateful to AcSIR for the doctoral registration (manuscript no.IICT/PUBS./2022/397).

Conflicts of Interest: The authors declare no conflict of interest.

References

1. Chen, J.; Li, X.; Wang, Y.; Huang, J.; Li, K.; Nie, X.; Jiang, J. Synthesis and application of environmental soybean oil-based epoxidized glycidyl ester plasticizer for poly(vinyl chloride). *Eur. J. Lipid Sci. Technol.* **2017**, *119*, 1600216. [[CrossRef](#)]
2. Duffy, E.; Gibney, M.J. Use of a food-consumption database with packaging information to estimate exposure to food-packaging migrants: Epoxidized soybean oil and styrene monomer. *Food Addit. Contam.* **2007**, *24*, 216–225. [[CrossRef](#)] [[PubMed](#)]
3. Wu, Q.; Hu, Y.; Tang, J.; Zhang, J.; Wang, C.; Shang, Q.; Feng, G.D.; Liu, C.; Zhou, Y.; Lei, W. High-Performance Soybean-Oil-Based Epoxy Acrylate Resins: “Green” Synthesis and Application in UV-Curable Coatings. *ACS Sustain. Chem. Eng.* **2018**, *6*, 8340–8349. [[CrossRef](#)]
4. Alagi, P.; Ghorpade, R.; Jang, J.H.; Patil, C.; Jirimali, H.; Gite, V.; Hong, S.C. Functional soybean oil-based polyols as sustainable feedstocks for polyurethane coatings. *Ind. Crops Prod.* **2018**, *113*, 249–258. [[CrossRef](#)]

5. Li, A.; Li, K. Pressure-Sensitive Adhesives Based on Epoxidized Soybean Oil and Dicarboxylic Acids. *ACS Sustain. Chem. Eng.* **2014**, *2*, 2090–2096. [[CrossRef](#)]
6. Javni, I.; Hong, D.P.; Petrović, Z.S. Polyurethanes from soybean oil, aromatic, and cycloaliphatic diamines by nonisocyanate route. *J. Appl. Polym. Sci.* **2012**, *128*, 566–571. [[CrossRef](#)]
7. Gholami, H.; Yeganeh, H. Soybean oil-derived non-isocyanate polyurethanes containing Azetidinium groups as antibacterial wound dressing membranes. *Eur. Polym. J.* **2020**, *142*, 110142. [[CrossRef](#)]
8. Hu, S.; Chen, X.; Torkelson, J.M. Bio-based Reprocessable Polyhydroxyurethane Networks: Full Recovery of Cross-link Density with Three Concurrent Dynamic Chemistries. *ACS Sustain. Chem. Eng.* **2019**, *7*, 10025–10034. [[CrossRef](#)]
9. Doley, S.; Bora, A.; Saikia, P.; Ahmed, S.; Dolui, S.K. Blending of cyclic carbonate based on soybean oil and glycerol: A non-isocyanate approach towards the synthesis of polyurethane with high performance. *J. Polym. Res.* **2021**, *28*, 146. [[CrossRef](#)]
10. Bähr, M.; Müllhaupt, R. Linseed and soybean oil-based polyurethanes prepared via the non-isocyanate route and catalytic carbon dioxide conversion. *Green Chem.* **2012**, *14*, 483–489. [[CrossRef](#)]
11. Yu, A.Z.; Setien, R.A.; Sahouani, J.M.; Docken, J.; Webster, D.C. Catalyzed non-isocyanate polyurethane (NIPU) coatings from bio-based poly(cyclic carbonates). *J. Coat. Technol. Res.* **2018**, *16*, 41–57. [[CrossRef](#)]
12. Mirzakhazadeh, Z.; Kosari, A.; Moayed, M.H.; Naderi, R.; Taheri, P.; Mol, J.M.C. Enhanced corrosion protection of mild steel by the synergetic effect of zinc aluminum polyphosphate and 2-mercaptobenzimidazole inhibitors incorporated in epoxy-polyamide coatings. *Corros. Sci.* **2018**, *138*, 372–379. [[CrossRef](#)]
13. Zhang, C.; Huang, K.C.; Wang, H.; Zhou, Q. Anti-corrosion non-isocyanate polyurethane polysiloxane organic/inorganic hybrid coatings. *Prog. Org. Coat.* **2020**, *148*, 105855. [[CrossRef](#)]
14. Wen, J.G.; Geng, W.; Geng, H.Z.; Zhao, H.; Jing, L.C.; Yuan, X.T.; Tian, Y.; Wang, T.; Ning, Y.J.; Wu, L. Improvement of Corrosion Resistance of Waterborne Polyurethane Coatings by Covalent and Noncovalent Grafted Graphene Oxide Nanosheets. *ACS Omega* **2019**, *4*, 20265–20274. [[CrossRef](#)]
15. Wu, Z.; Tang, L.; Dai, J.; Qu, J. Synthesis and properties of fluorinated non-isocyanate polyurethanes coatings with good hydrophobic and oleophobic properties. *J. Coat. Technol. Res.* **2019**, *16*, 1233–1241. [[CrossRef](#)]
16. Hamidon, T.S.; Yun, T.P.; Zakaria, F.A.; Hussin, M.H. Potential of zinc based-graphene oxide composite coatings on mild steel in acidic solution. *J. Indian Chem. Soc.* **2021**, *98*, 100243. [[CrossRef](#)]
17. Asemani, H.R.; Mannari, V.V. Dual-curable coatings obtained from multi-functional non-isocyanate polyurethane oligomers. *J. Coat. Technol. Res.* **2022**, *5*, 1393–1407. [[CrossRef](#)]
18. Doley, S.; Dolui, S.K. Solvent and catalyst-free synthesis of sunflower oil based polyurethane through non-isocyanate route and its coatings properties. *Eur. Polym. J.* **2018**, *102*, 161–168. [[CrossRef](#)]
19. Kathalewar, M.; Sabnis, A.; Waghoo, G. Effect of incorporation of surface treated zinc oxide on non-isocyanate polyurethane based nano-composite coatings. *Prog. Org. Coat.* **2013**, *76*, 1215–1229. [[CrossRef](#)]
20. Micić, D.; Šljukić, B.; Zujovic, Z.; Travas-Sejdic, J.; Ćirić-Marjanović, G. Electrocatalytic Activity of Carbonized Nanostructured Polyanilines for Oxidation Reactions: Sensing of Nitrite Ions and Ascorbic Acid. *Electrochim. Acta* **2014**, *120*, 147–158. [[CrossRef](#)]
21. Pakapongpan, S.; Mensing, J.P.; Phokharatkul, D.; Lomas, T.; Tuantranont, A. Highly selective electrochemical sensor for ascorbic acid based on a novel hybrid graphene-copper phthalocyanine-polyaniline nanocomposites. *Electrochim. Acta* **2014**, *133*, 294–301. [[CrossRef](#)]
22. Rana, U.; Paul, N.D.; Mondal, S.; Chakraborty, C.; Malik, S. Water soluble polyaniline coated electrode: A simple and nimble electrochemical approach for ascorbic acid detection. *Synth. Met.* **2014**, *192*, 43–49. [[CrossRef](#)]
23. Xue, C.; Wang, X.; Zhu, W.; Han, Q.; Zhu, C.; Hong, J.; Zhou, X.; Jiang, H. Electrochemical serotonin sensing interface based on double-layered membrane of reduced graphene oxide/polyaniline nanocomposites and molecularly imprinted polymers embedded with gold nanoparticles. *Sens. Actuators B Chem.* **2014**, *196*, 57–63. [[CrossRef](#)]
24. Zhou, C.; Shi, Y.; Luo, J.; Zhang, L.; Xiao, D. Diameter-controlled synthesis of polyaniline microtubes and their electrocatalytic oxidation of ascorbic acid. *J. Mater. Chem. B* **2014**, *2*, 4122–4129. [[CrossRef](#)]
25. Wu, T.; Wang, L.Y.; Du, S.; Guo, W.J.; Pei, M.S. Micro/nanostructures of PANI obtained in the presence of water soluble polymers and their electrochemical sensing properties. *RSC Adv.* **2015**, *5*, 69067–69074. [[CrossRef](#)]
26. Shanmugasundaram, K.; Sai-Anand, G.; Gopalan, A.I.; Lee, H.G.; Yeo, H.K.; Kang, S.W.; Lee, K.P. Direct electrochemistry of cytochrome c with three-dimensional nanoarchitected multicomponent composite electrode and nitrite biosensing. *Sens. Actuators B Chem.* **2016**, *228*, 737–747. [[CrossRef](#)]
27. Wei, Y.; Yang, C.; Ding, T. A one-step method to synthesize N,N'-bis(4'-aminophenyl)-1,4-quinonediimine and its derivatives. *Tetrahedron Lett.* **1996**, *37*, 731–734. [[CrossRef](#)]
28. Chen, L.; Yu, Y.; Mao, H.; Lu, X.; Zhang, W.; Wei, Y. Synthesis of parent aniline tetramer and pentamer and redox properties. *Mater. Lett.* **2005**, *59*, 2446–2450. [[CrossRef](#)]
29. Peng, C.W.; Hsu, C.; Lin, K.H.; Li, P.L.; Hsieh, M.F.; Wei, Y.; Yeha, J.M.; Yuc, Y.H. Electrochemical corrosion protection studies of aniline-capped aniline trimer-based electroactive polyurethane coatings. *Electrochim. Acta* **2011**, *58*, 614–620. [[CrossRef](#)]
30. Huang, K.Y.; Shiu, C.L.; Wu, P.S.; Wei, Y.; Yeh, J.M.; Li, W.T. Effect of amino-capped aniline trimer on corrosion protection and physical properties for electroactive epoxy thermosets. *Electrochim. Acta* **2009**, *54*, 5400–5407. [[CrossRef](#)]
31. Weng, C.J.; Huang, J.Y.; Huang, K.Y.; Jhuo, Y.S.; Tsai, M.H.; Yeh, J.M. Advanced anticorrosive coatings prepared from electroactive polyimide-TiO₂ hybrid nanocomposite materials. *Electrochim. Acta* **2010**, *55*, 8430–8438. [[CrossRef](#)]

32. Huang, T.C.; Yeh, T.C.; Huang, H.Y.; Ji, W.F.; Lin, T.C.; Chen, C.A.; Yang, T.I.; Yeh, J.M. Electrochemical investigations of the anticorrosive and electrochromic properties of electroactive polyamide. *Electrochim. Acta* **2012**, *63*, 185–191. [[CrossRef](#)]
33. Yeh, L.C.; Huang, T.C.; Huang, Y.P.; Huang, H.Y.; Chen, H.H.; Yang, T.I.; Yeh, J.M. Synthesis electroactive polyurea with aniline-pentamer-based in the main chain and its application in electrochemical sensor. *Electrochim. Acta* **2013**, *94*, 300–306. [[CrossRef](#)]
34. Ji, W.F.; Chu, C.M.; Hsu, S.C.; Lu, Y.D.; Yu, Y.C.; Santiago, K.S.; Yeh, J.M. Synthesis and characterization of organo-soluble aniline oligomer-based electroactive doped with gold nanoparticles, and application to electrochemical sensing of ascorbic acid. *Polymer* **2017**, *128*, 218–228. [[CrossRef](#)]
35. Heng, Z.G.; Zhang, X.; Chen, Y.; Zou, H.; Liang, M. In-situ construction of “octopus”-like nanostructure to achieve high performance epoxy thermosets. *Chem. Eng. J.* **2019**, *360*, 542–552. [[CrossRef](#)]
36. Bouoidina, A.; Ech-chihbi, E.; El-Hajjaji, F.; El Ibrahim, B.; Kaya, S.; Taleb, M. Anisole derivatives as sustainable-green inhibitors for mild steel corrosion in 1 M HCl: DFT and molecular dynamic simulations approach. *J. Mol. Liq.* **2021**, *324*, 115088. [[CrossRef](#)]
37. Ma, Y.; Ye, Y.; Wan, H.; Chen, L.; Zhou, H.; Chen, J. Chemical Modification of Graphene Oxide to Reinforce the Corrosion Protection Performance of UV-Curable Polyurethane Acrylate Coating. *Prog. Org. Coat.* **2020**, *141*, 105547. [[CrossRef](#)]
38. Xing, C.; Zhang, Z.; Yu, L.; Zhang, L.; Bowmaker, G.A. Electrochemical Corrosion Behaviour of Carbon Steel Coated by Polyaniline Copolymers Micro/Nanostructures. *RSC Adv.* **2014**, *4*, 32718–32725. [[CrossRef](#)]
39. Yongbo, D.; Liang, J.; Liu, G.; Ni, W.; Shen, L. Preparation and Anticorrosive Property of Soluble Aniline Tetramer. *Coatings* **2019**, *9*, 399.

Disclaimer/Publisher’s Note: The statements, opinions and data contained in all publications are solely those of the individual author(s) and contributor(s) and not of MDPI and/or the editor(s). MDPI and/or the editor(s) disclaim responsibility for any injury to people or property resulting from any ideas, methods, instructions or products referred to in the content.